ADVANCED MATERIALS

or plasma, as can be seen in Figures 3,4, so that we cannot apply a similar model.

When using an electron beam instead of an ion beam, the CNTs could not be aligned, which indicates that the mass of the charge carrier is possibly involved in the process.

The CNT aligned by this method maintains its elasticity, as is observed in the bending test with a nanomanipulator installed in the scanning electron microscope. Furthermore, we could obtain stable SFM images with the aligned CNT tip.[19]

We believe the impact of our findings will not be limited to the field of SFM. In general, the alignment of CNTs is a crucial issue for their testing and application. So far, several processes have been reported, including cutting a polymer resin/CNT composite,[20] rubbing CNT films,[21] and electrophoresis.[22] These are mechanical and electrical methods, where CNTs are aligned in groups on a surface. The new method described here is unique since it can treat individual CNTs in space (vacuum) and use the interaction with the beams of charged particles.

The understanding and knowledge of the process reported here is preliminary and far from complete. Future work should investigate the ion beam/CNT interaction, the structure and properties of the CNT after irradiation with the FIB, and the development of new experiments and applications that are enabled by this process.

Received: June 15, 2005
Final version: July 12, 2005
Published online: November 21, 2005

[1] S. Iijima, *Nature* **1991**, *354*, 56.
[2] M. S. Dresselhaus, G. Dresselhaus, P. C. Eklund, *Science of Fullerenes and Carbon Nanotubes*, Academic Press, New York **1996**.
[3] C. Dekker, *Phys. Today* **1999**, *May*, 22.
[4] H. Dai, J. H. Hafner, A. G. Rinzler, D. T. Colbert, R. E. Smalley, *Nature* **1996**, *384*, 147.
[5] A. Sawada, M. Iriguchi, W. J. Zhao, C. Ochiai, M. Takai, *J. Vac. Sci. Technol. B* **2003**, *21*, 362.
[6] T. Uchihashi, N. Choi, M. Tanigawa, M. Ashino, Y. Sugawara, H. Nishijima, S. Akita, Y. Nakayama, H. Tokumoto, K. Yokoyama, S. Morita, M. Ishikawa, *Jpn. J. Appl. Phys., Part 2* **2000**, *39*, 887.
[7] T. D. Yuzvinsky, A. M. Fennimore, W. Mickelson, C. Esquivias, A. Zettl, *Appl. Phys. Lett.* **2005**, *86*, 053 109.
[8] E. Yenilmez, Q. Wang, R. J. Che, D. Wang, H. Dai, *Appl. Phys. Lett.* **2002**, *80*, 2225.
[9] Y. C. Chang, D. C. Wang, C. S. Chang, T. T. Tsong, *Appl. Phys. Lett.* **2003**, *82*, 3541.
[10] W. S. Song, K. Y. Jung, B. O, B. C. Park, *Rev. Sci. Instrum.* **2005**, *76*, 025 107.
[11] T. W. Ebbesen, P. M. Ajayan, *Nature* **1992**, *358*, 220.
[12] T. W. Ebbesen, P. M. Ajayan, H. Hlura, K. Tanigaki, *Nature* **1994**, *367*, 519.
[13] Y. Martin, H. K. Wickramasinghe, *Appl. Phys. Lett.* **1994**, *64*, 2498.
[14] D. Halliday, R. Resnick, *Fundamentals of Physics*, 5th ed., John Wiley & Sons, New York **1998**.
[15] C. Bower, W. Zhu, S. Jin, O. Zhou, *Appl. Phys. Lett.* **2000**, 77, 830.
[16] J. F. AuBuchon, L.-H. Chen, S. Jin, *J. Phys. Chem. B* **2005**, *109*, 6044.
[17] Y. Wei, C. Xie, K. A. Dean, B. F. Coil, *Appl Phys. Lett.* **2001**, *79*, 4527.
[18] H. Lee, D. Kim, C. Kim, H. Jang, *J. Inform. Display* **2003**, *4*, 35.
[19] B. C. Park, K. Y. Jung, J. Hong, W. Y. Song, B. O, J. A. Kim, *Proc. SPIE* **2005**, *5752*, 412.
[20] P. M. Ajayan, O. Stephan, C. Colliex, D. Trauth, *Science* **1994**, *265*, 1212.
[21] W. A. Heer, W. S. Bacsa, A. Chatelain, T. Geftin, R. Humphrey-Baker, L. Forro, D. Ugarte, *Science* **1995**, *268*, 845.
[22] K. Yamamoto, S. Akita, Y. Nakayama, *Jpn. J. Appl. Phys., Part 2* **1996**, *35*, L917.

DOI: 10.1002/adma.200500912

Photocurrent Amplification at Carbon Nanotube–Metal Contacts**

By *Der-Hsien Lien*, *Wen-Kuang Hsu*,* *Hsiao-Wen Zan*, *Nyan-Hwa Tai*, and *Chuen-Horng Tsai*

Single-walled carbon nanotubes (SWNTs) are promising electronic materials and have been fabricated into various nanodevices, such as sensors for dipolar molecules and field-effect transistors (FETs).[1,2] Recently, the study of carbon nanotube (CNT) FETs has focused on current modulation by gate control.[3,4] Carbon nanotubes brought into contact with metals form Schottky barriers, and the metal Fermi level (E_F) falls to the mid-bandgap value of the CNTs, resulting in the formation of ambipolar FETs.[5,6] Heinze et al. have constructed various contact geometries and have realized that sharper contact structures lead to electric-field enhancement in the Schottky region, and thus a higher current is produced at a lower threshold voltage.[7] This result suggests that the electrostatic potential within nanotubes is highly sensitive to external electric fields at the junction region. Meanwhile, the contact potential varies with surface polarization owing to O_2 absorption, leading to an asymmetric current–voltage (I–V) profile at zero gate voltage.[8] In this work, we demonstrate photocurrent generation at SWNT–electrode contacts at zero bias. This current can be significantly amplified by a factor of 4–7 under bias-voltage operation. It has also been found that the generation of current is faster under negative bias than at positive bias voltages by a factor of 6–7. The above phenome-

[*] Prof. W.-K. Hsu, D.-H. Lien, Prof. N.-H. Tai
Department of Materials Science and Engineering
National Tsing Hua University
Hsinchu 30013 (Taiwan)
E-mail: wkhsu@mx.nthu.edu.tw
Prof. H.-W. Zan
Department of Photonics
National Chiao Tung University
Hsinchu 30010 (Taiwan)
Prof. C.-H. Tsai
Department of Engineering and System Science
National Tsing Hua University
Hsinchu 30013 (Taiwan)

[**] We thank the National Science Council of Taiwan for financial support (NSC 93-2113-M-007-028) and UST-CNST project.

non resembles the behaviour of conventional Si-based Schottky diodes, and the underlying mechanism involves reduction of the barrier height and widening of the depletion region upon application of a bias.

In order to minimize heating at the film–electrode contacts owing to infrared radiation, and O_2 desorption from SWNTs by UV-light exposure, a green laser with an energy of 5 mW has been employed as the illumination source. In-situ measurements of photocurrent have been made by two different methods. First, photocurrent is collected as a result of targeting the beam on the film and electrodes A and B, with and without bias control (Figs. 1a–c). Secondly, the beam is consecutively shifted from electrodes A to B, and then towards C, and current collection is carried out under positive and negative bias, respectively (Fig. 2a). In our experiments, the bias voltage across electrodes A and B (V_{bias} A–B) and across electrodes B and A (V_{bias} B–A) are defined as positive and negative bias, respectively. The probe C is electrically connected to the ground.

When the beam is focused only on the film at zero bias, no distinguishable photocurrent is collected (Fig. 1b), whereas a noticeable current has been detected when the beam is targeted on both electrodes (Figs. 1a,c). The profile shows a mirror symmetry, and the current collected at electrodes A and B are of a similar magnitude, ~0.18 μA (Fig. 1e). Interestingly, when the beam is targeted on either A or B at 0.8 mV bias, the current is immediately increased to 0.8 and 1.2 μA, respectively (Fig. 1f); values which are a factor of 4–6 higher than currents depicted in Figure 1e. Repeat experiments on different samples exhibit similar results. Figures 2a,b show photocurrent production as a function of successive beam shift from electrode A to C at 0.5 mV. The current generated is 1 μA at electrode A (panel 1), and decays with spot movement to position 2 by ~0.5 μA (panels 1,2, Fig. 2b). A larger negative current (–1.4 μA) is re-established as the beam moves on to electrode B (panels 3,4, Fig. 2b). The current again decreases when the beam shifts from B towards C, and the current produced at positions 5 and 6 are 0.8 and 0.6 μA, respectively (panels 5,6). Figure 2b indicates that a) a higher current is obtained when the beam is focused on the film–electrode contact rather than on the film, and b) a higher current is always produced by the laser beam at the electrode which is at a negative bias. These two observations have been verified by repetitive experiments on different SWNT films. It is thus clear that illumination by the laser is responsible for the higher current generation seen in this contact structure. Accordingly, it is important to characterize the nature of the SWNT–electrode contact. We have carried out aerial measurements of thermal electric power (TEP) on the nanotube sample, and the Seebeck coefficient is positive (51.3 $\mu V K^{-1}$), which indicates that the SWNTs are a p-type material, and that the contacts are of a metal/p-doped semiconductor type. In other words, the SWNT–film hung between Zn electrodes is equivalent to two Schottky diodes connected opposite to each other (Fig. 1d). Classical photodiodes consist of a p–n junction operating under negative bias, and the photocurrent always flows from n to p. When our system is positively biased (V_{bias} A–B), with the beam focused on electrode B, the photocurrent is generated at electrode B and flows towards A, because B is at a negative bias with respect to A (upper panel, Fig. 1d). A similar situation occurs for V_{bias} B–A, the photocurrent is produced at electrode A, and flows towards B (lower panel, Fig. 1d). Thus the higher current with a minus sign seen in Figure 2b (panels 3,4) corresponds to Figure 1d (upper panel). Photocurrent generation in our Schottky contact increases with light intensity by ~0.04 $\mu A mW^{-1}$, and the maximum photocurrent reaches 1.4 μA. The quantum efficiency (η_{ph}) and responsivity (S) have been calculated to be 0.093–0.1 % and 0.04–0.06 $\% A W^{-1}$, respectively; the latter is much lower than values for Si-based photodiodes illuminated by the same excitation energy ($S = 30\ \% A W^{-1}$). The low S is understandable because the population of semiconducting SWNTs in thin films is essentially limited, and screening effects of the neighboring metallic SWNTs reduces the exciton density in the deple-

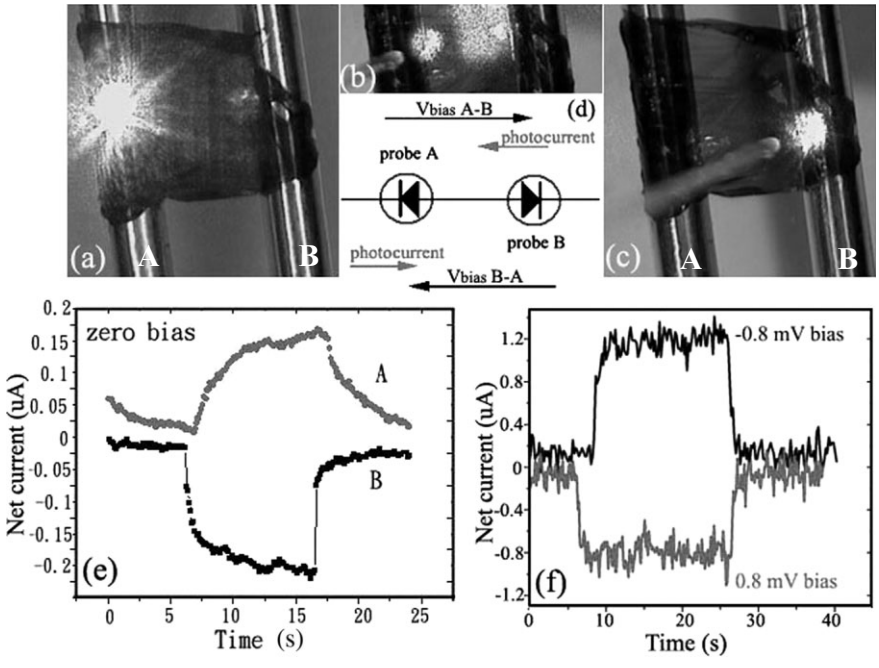

Figure 1. A green laser spot a) on electrode A, b) on the film, and c) on electrode B. d) Two photodiodes connected opposite to one another. e) The corresponding photocurrent versus time obtained for (a–c) at zero bias, and f) the corresponding photocurrent versus time profile obtained for (a–c) at ±0.8 mV bias voltage. The sharp increases/decreases in photocurrent correspond to movement of the beam between the positions indicated in (a–c).

ADVANCED MATERIALS

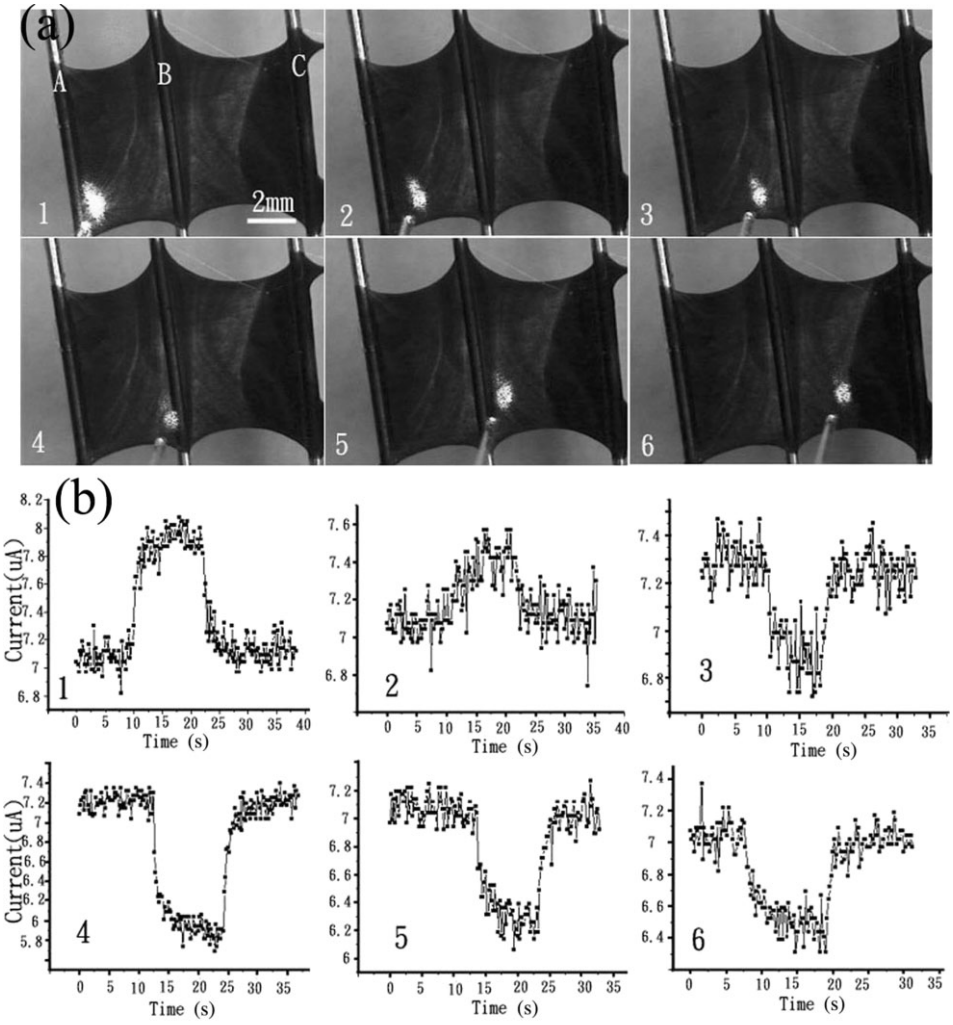

Figure 2. a) The beam spot shifts from electrode A to B (grounded electrode) and towards C, and b) the corresponding photocurrents that are established.

tion region.[9] Previous workers have carried out similar experiments on a single SWNT and have realized a higher quantum efficiencies ($\eta_{ph} > 10\,\%$).[10] This outcome is mainly a result of the strong electric field established in short nanotubes that efficiently separates more e–h (electron–hole) pairs. When a SWNT film is hung between electrodes, the electric field becomes apparent only at regions near the contact. Photocurrent generation at positions 5 and 6 is interesting (Fig. 2b), and can be regarded as a third photodiode connected in series with electrodes A and B, under V_{bias} A–C.

As-made SWNTs are essentially O_2-saturated, and the adsorbed molecules can be considered to be an intermediate layer between the tubes and the electrodes.[11] The attached molecules enhance the tube surface dipole, and the electrons are therefore strongly confined in the SWNTs, resulting in a stronger electron affinity. This description is further supported by the presence of a high specific contact resistance in our devices. An ideal Schottky contact has R_c below $m\Omega\,cm^2$, and here we have obtained $R_c = 30$–$50\ \Omega\,cm^2$. Consequently, carrier passage through Schottky barriers must rely on tunneling processes. According to Yu's model, the type of carrier transmission through a barrier can be determined based on Equation 1:[12]

$$E_{tunneling} = 18.5 \times 10^{-15}[N/(m^*/m)\varepsilon]^{1/2}\ \text{eV} \quad (1)$$

where $E_{tunneling}$ is the tunneling electron through the Schottky barrier with energy equivalent to the bottom of the conduction band in the depletion region, N is the doping concentration, and ε and m^*/m are the permittivity and effective mass of SWNTs, respectively. Since electron tunneling through a barrier is dependent upon temperature, the $qE_{tunneling}/k_BT$ (q: electron charge: k_B: Boltzmann constant; T: temperature) ratio is normally used to indicate the type of carrier passage through the barrier. If $qE_{tunneling}/kT \ll 1$ the transport is thermionic emission, and for $qE_{tunneling}/kT \geq 1$ the mechanism is field emission. Here the N value needs to be estimated in order to obtain the $E_{tunneling}$ value. The carrier density of

metallic SWNTs is $\sim 8 \times 10^{18}$ cm^{-3}, as measured using solution-phase electron paramagnetic resonance (EPR) spectroscopy.[13] This value is comparable with that of multiwalled CNTs (1×10^{18}–10^{19} cm^{-3}).[14] O_2-saturated bulk SWNTs show a 10–15 % decrease in resistance compared with the value obtained in vacuum, and this has been attributed to the introduction of metallic properties in semiconducting tubes by O_2 doping.[15] Calculations reveal that each spin-triplet molecule extracts 10 % of the electrons from semiconducting nanotubes and the doping concentration N can be inferred based on

$$N_{\text{total}} = N^2 \exp(-E_d/2k_B T) \quad (2)$$

where the total carrier density N_{total} is set at 10^{18} cm^{-3}, the ionization energy of oxygen E_d is 0.16 eV, and the thermal energy $k_B T$ is 26 meV. Thus, N is roughly around 10^{16} cm^{-3}. By substituting N into Equation 1, we obtain $qE_{\text{tunneling}}/kT \sim 8 \times 10^{-24}$, indicating a thermionic emission model for the present study. The intermediate O_2 has a negative effect on the electric-field build-up at the depletion region; specifically, tunneling electrons are trapped by O_2 owing to so-called charge neutralization. Accordingly, the strength of the electric field ($\boldsymbol{E}$) at the depletion layer, which is usually determined from the potential drop across the junction (V_d), is therefore anticipated to be lower, compared with perfect contact devices.[11] The relationship between $\boldsymbol{E}$ and V_d is written as

$$\boldsymbol{E} = \sqrt{2qNV_d/\varepsilon} \quad (3)$$

By setting $\varepsilon = 25$ and $N = 1 \times 10^{16}$, we obtain $\boldsymbol{E} = \sqrt{1.28 \times 10^{-3} V_d}$. For conventional Si-based Schottky devices, V_d is 0.5 V. If one considers a similar value for the present study, $\boldsymbol{E}$ appears to be 0.025 V m^{-1}. This value is comparable with classical devices and is responsible for photocurrent generation at zero bias, i.e., the photovoltaic effect. Work functions of Zn and an ideal (10,10) SWNT are 4.35 eV and 4.5 eV, respectively,[16,17] which means that the equalized Fermi level lies approximately between the mid-gap and valence-band edge of SWNTs in the junction region. The barrier height can therefore be evaluated according to Equation 4

$$\phi_b = E_g - \phi_M + \phi_e + \Delta U \quad (4)$$

where ϕ_M and ϕ_e are workfunctions of the metal and SWNT electron affinity, respectively, and ΔU is the diffusion potential ($\sim$0.15 eV).[11] The electron affinity of SWNTs has been estimated to be 2.84 eV and 4.18 eV, based on (5,0) and (16,0) CNT models, respectively;[18,19] the latter value seems to be more reasonable because ϕ_e increases upon exposure to adsorbed molecules and the current samples approximate (16,0) tubes. When $\phi_e = 4.18$ eV is used, we obtain $\phi_b = 0.48$ eV. This value is higher than individual SWNT Schottky devices by 0.1 eV, whereas it supports previous conclusions that the increased ϕ_b upon O_2 doping can prevent electrons from being injected into the junction.[3] In other words, the current collected in Figures 1e,f truly originates from photoexcitation at the tube–metal junction. Current generation at electrodes as a result of laser heating (i.e., thermoelectric power) is unlikely, because such a current cannot be amplified via bias-voltage modulation.

Three factors can lead to the bias dependence of photocurrent production seen in Figures 1f,2; namely, a) widening of the depletion layer, b) effect of the O_2 interfacial layer, and c) reduction of ϕ_b. The second factor can be immediately ruled out as our junction devices rely on an emission mechanism. Widening of the depletion layer only occurs in p–n junctions under reverse characteristics, thus the increase of the photocurrent by bias voltage must be caused by the third factor. The decrease in ϕ_b upon the application of a bias is directly related to image forces at the junction interface. The image force means that electron transmission through the barrier is accelerated by counter charges at the opposite surface, and the image potential reduces the barrier height. The initial barrier height (ϕ_b) therefore needs to be modified to an effective barrier height,

$$\phi_e = \phi_b - \phi_i \quad (5)$$

where ϕ_i is the barrier lowering resulting from the image force. The intermediate O_2 layer together with the image force complicates the interfacial characteristics, and thus the initial model for current passage through the barrier

$$J = J_o[\exp(qV_{\text{bias}}/kT) - 1] \quad (6)$$

needs to be revised. The amended model involves an ideality factor and an effective mass in order to justify the relationship between the current density through the barrier and V_{bias}

$$J = J_o[\exp(qV_{\text{bias}}/nkT)][1 - \exp(-qV_{\text{bias}}/kT)] \quad (7)$$

where

$$J_o = AT^2 \exp(-q\phi_b/kT) \quad (8)$$

and A is the Richardson constant corresponding to the effective mass in semiconductors ($= 1.2 \times 10^6 (m^*/m)$), n is the ideality factor, and

$$1/n = 1 - \partial\phi_e/\partial V \quad (9)$$

Equation 7 indicates that the effective mass plays a crucial role in determining current generation upon bias application, and that the ideality factor is indicative of system characteristics. For a small n value, devices are usually regarded to have an ideal contact structure and the I–V profile is linear. Larger values of n imply the presence of an intermediate layer between the metal/semiconductor interface. Since the effective mass varies with tube diameter, the ideality factor (n) for the current devices can be calculated by plotting $\ln\{J/[1 - \exp(-qV/kT)]\}$ against V_{bias} over different m^*/m.[18] Figure 3a shows larger fluctuations above 0.5 mV and below –0.5 mV, indicating that the ideality factor is not a constant in both regions,

ADVANCED MATERIALS

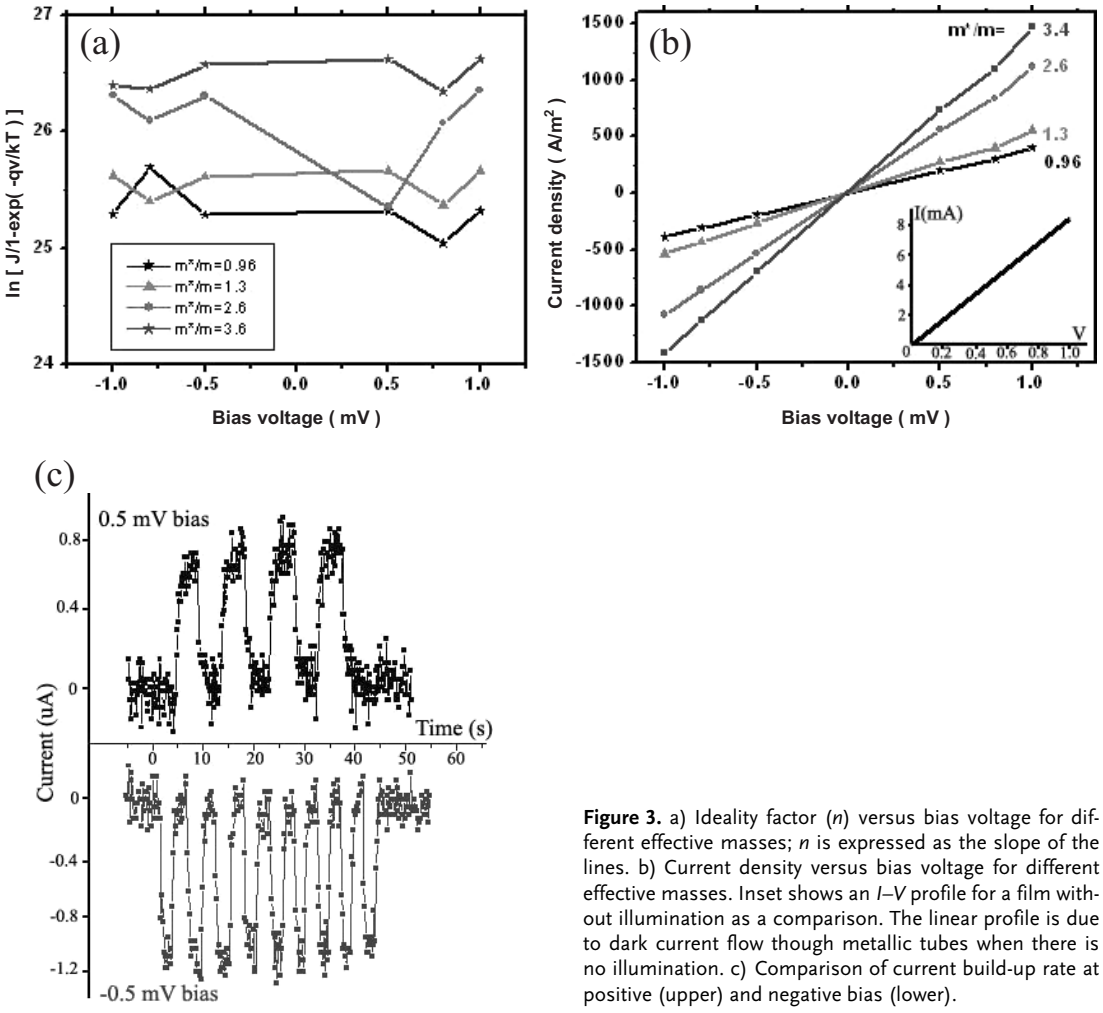

Figure 3. a) Ideality factor (*n*) versus bias voltage for different effective masses; *n* is expressed as the slope of the lines. b) Current density versus bias voltage for different effective masses. Inset shows an *I–V* profile for a film without illumination as a comparison. The linear profile is due to dark current flow though metallic tubes when there is no illumination. c) Comparison of current build-up rate at positive (upper) and negative bias (lower).

and thus the photocurrent increases with a higher V_{bias} in the Schottky junction in a nonlinear manner. This is understandable because a higher bias enhances charge accumulation at the absorbed O_2 layers between the SWNTs and the Zn surface, and thus the junction behaves as a plate-to-plate capacitor in some respects. Between ±0.5 mV the ideality factor only deviates slightly, indicating a stable current amplification upon bias ramping. This effect is interesting and has not been previously reported, as the photocurrent can still be amplified linearly between ±0.5 mV in the presence of the oxide layer. Figure 3b shows the current-density-versus-bias profile, which reveals a linear current increment with V_{bias} ramping, and a greater current increment at a larger effective mass, consistent with Figure 3a. The inset to Figure 3b shows an *I–V* profile without illumination as a comparison. A larger effective mass means a greater density of states near the valence-band edge, and thus the tunneling probability through the junction increases and the current is increased.[19] It is unlikely that the increase in current and tunneling probability occurs as a result of extra tunneling via metal/vacuum/metallic–SWNTs (note that metallic SWNTs are also in contact with the electrodes), as the work functions of metallic SWNTs (4.5 eV) and Zn (4.35 eV) are significantly greater than the barrier height ($\phi_b = 0.48$ eV). The higher current collected at negative bias is clearly a result of the widening of the depletion region (Fig. 1f, position 4 in Fig. 2), because more photocarriers are produced when the depletion layer is widened (note that in a photodiode, e–h pairs are only separated in the depletion region).

The rate of photocurrent build-up at the SWNT–Zn contact has been compared at positive and negative bias. Figure 3c shows a profile of current creation versus time-dependent-illumination at 0.5 mV (top) and at –0.5 mV (lower panel). The corresponding current and build-up rate are 0.8 μA at 0.5 μA s^{-1} and 1.4 μA at 0.08 μA s^{-1}, respectively; the latter is faster than the former by a factor of 6–7, and the overall current switching occurs on a scale of milliseconds. The faster and higher current build-up at negative bias is attributed to an

enhanced photovoltaic effect, because more e–h pairs are separated by the electric field in the widening region.

In summary, photocurrent has been produced at SWNT–Zn contacts with zero bias. This current is amplified by a factor of 4–7 upon application of a bias, and higher currents are always achieved at the electrode opposite to that with positive bias. Between ±0.5 mV biases, the ideality factor only deviates slightly and the current increment scales linearly with bias ramping. Nonlinear current amplification emerges above 0.5 mV and below –0.5 mV, owing to charge accumulation at the interfacial O_2 layer. Carrier passage through the junction is essentially tunneling-type and device switching is of the order of milliseconds. The current build-up at negative bias is faster by a factor of 6–7 over that of positive-bias operation.

Experimental

SWNTs were made by the pyrolysis of a mixture containing ferrocene, benzene, and thiophene in the presence of H_2 [20]. The as-made materials were cotton-like and consisted of networked and tangled SWNT ropes, with the SWNT diameter being around 1.1–2 nm. The relationship between the diameter of semiconducting SWNTs and the photoexcitation energy has been discussed previously, and peaks were observed at 0.6 and 1.3 eV, corresponding to E_{1-1} and E_{2-2} transitions, respectively [9,21]. We found that on dispersing the cotton-like sample (50 mg) in acetone (100 mL) by using a ultrasonic probe for 10 min, thin films of SWNTs separated out from the bulk. We have extracted these thin films and transferred them onto two aligned Zn electrodes using pipettes. When the acetone solution was dried, the SWNT film appeared to be hung between the electrodes (Fig. 4a). The film thickness was ~200–400 nm, determined by α-step (Fig. 4b), and the film resistance changed from sample to sample, usually between 100 and 800 Ω.

Received: May 4, 2005
Final version: August 9, 2005
Published online: November 15, 2005

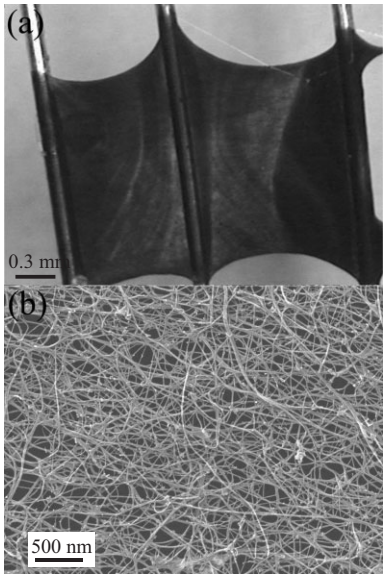

Figure 4. a) A SWNT film hung between Zn electrodes, and b) a scanning electron microscopy image of SWNTs.

[1] P. G. Collins, K. Bradley, M. Ishigami, A. Zettl, *Science* **2000**, *287*, 1801.
[2] S. J. Tans, A. R. M. Verschueren, C. Dekker, *Nature* **1998**, *393*, 49.
[3] V. Derycke, R. Martel, J. Appenzeller, P. Avouris, *Appl. Phys. Lett.* **2002**, *80*, 2773.
[4] A. Rochefort, M. D. Ventra, P. Avouris, *Appl. Phys. Lett.* **2001**, *78*, 2521.
[5] F. Léonard, J. Tersoff, *Phys. Rev. Lett.* **2000**, *84*, 4693.
[6] A. A. Odintsov, *Phys. Rev. Lett.* **2000**, *85*, 150.
[7] S. Heinze, J. Tersoff, R. Martel, V. Derycke, J. Appenzeller, P. Avouris, *Phys. Rev. Lett.* **2002**, *89*, 106 801.
[8] M. Shim, G. P. Siddons, *Appl. Phys. Lett.* **2003**, *83*, 3564.
[9] H. M. Cheng, F. Li, X. San, S. D. M. Brown, M. A. Pimenta, A. Marucci, G. Dresselhaus, M. S. Dresselhaus, *Chem. Phys. Lett.* **1998**, *289*, 602.
[10] S. M. Bachilo, M. S. Strano, C. Kittrell, R. H. Hauge, R. E. Smalley, R. B. Weisman, *Science* **2002**, *298*, 2361.
[11] I. A. Levitsky, W. B. Euler, *Appl. Phys. Lett.* **2003**, *83*, 1857.
[12] M. Freitag, Y. Martin, J. A. Misewich, R. Martel, P. Avouris, *Nano Lett.* **2003**, *3*, 1067.
[13] T. Yamada, *Phys. Rev. B: Condens. Matter* **2004**, *69*, 125 408.
[14] A. Y. C. Yu, *Solid-State Electron.* **1970**, *13*, 239.
[15] Y. Chen, J. Chen, H. Hu, M. A. Hamon, M. E. Itkis, R. C. Haddon, *Chem. Phys. Lett.* **1999**, *299*, 532.
[16] G. Baumgartner, M. Carrard, L. Zuppiroli, W. Bacsa, W. A. de Heer, L. Forró, *Phys. Rev. B: Condens. Matter* **1997**, *55*, 6704.
[17] P. G. Collins, K. Bradley, M. Ishigami, A. Zettl, *Science* **2000**, *287*, 1801.
[18] M. Akbi, A. Lefort, *J. Phys. D: Appl. Phys.* **1998**, *31*, 1301.
[19] Y. Xue, M. A. Ratner, *Appl. Phys. Lett.* **2003**, *83*, 2429.
[20] V. Perebeinos, J. Tersoff, P. Avouris, *Phys. Rev. Lett.* **2004**, *92*, 257 402.
[21] D. A. Stewart, F. Léonard, *Phys. Rev. Lett.* **2004**, *93*, 107 401.

DOI: 10.1002/adma.200500951

High, Purely Electrostrictive Strain in Lead-Free Dielectrics

By *Chen Ang** and *Zhi Yu*

It is known that a dielectric will change its dimensions under an applied electric field, where its strain (S) is expressed by a quadratic term of the polarization (P), $S = Q \cdot P^2$, called the electrostrictive effect, where Q is the electrostrictive coefficient. This effect is very weak in most materials, with the strain level far below 0.1 % and a very small Q.[1,2] However, in some ferroelectric relaxors,[3,4] the electrostrictive strain is practically useful owing to its high level of 0.1 % and Q value of ~10^{-2} m^4C^{-2}. Compared with the piezoelectric effect, the electrostrictive effect has several unique advantages—posses-

[*] Prof. C. Ang, Dr. Z. Yu
Department of Physics, The University of Akron
Akron, OH 44325 (USA)
E-mail: angchen@physics.uakron.edu